

A Deep Keck/NIRC2 Search for Thermal Emission from Planetary Companions Orbiting Fomalhaut

Thayne Currie¹, Ryan Cloutier¹, John H. Debes², Scott J. Kenyon³, Denise Kaisler⁴

ABSTRACT

We present deep Keck/NIRC2 1.6 and 3.8 μm imaging of Fomalhaut to constrain the near-infrared (IR) brightness of Fomalhaut b, recently confirmed as a likely planet (Currie et al. 2012a), and search for additional planets at $r_{proj} = 15\text{--}150\text{ AU}$. Using advanced/novel PSF subtraction techniques, we identify seven candidate substellar companions Fomalhaut b-like projected separations. However, multi-epoch data shows them to be background objects. We set a new $3\text{-}\sigma$ upper limit for Fomalhaut b's H -band brightness of $m(H) \sim 23.15$ or $1.5\text{--}4.5 M_J$. We do not recover the possible point source reported from Spitzer/IRAC data: at its location detection limits are similar to those for Fomalhaut b. Our data when combined with other recent work rule out planets with masses and projected separations comparable to HR 8799 bcde and $M > 3 M_J$ planets at $r_{proj} > 45\text{ AU}$. The *James Webb Space Telescope* will likely be required to shed substantial further light on Fomalhaut's planetary system in the next decade.

Subject headings: planetary systems, stars: early-type, stars: individual: Fomalhaut

1. Introduction

The nearby A star Fomalhaut has long been suspected of harboring a planetary system, given its bright, dusty Kuiper belt-like debris ring (Aumann et al. 1985; Stapelfeldt et al. 2004; Acke et al. 2012) whose pericenter offset from the star is consistent with dynamical sculpting from an embedded planet (Kalas et al. 2005). Using the *Hubble Space Telescope's*

¹University of Toronto

²Space Telescope Science Institute

³Harvard-Smithsonian Center for Astrophysics

⁴Citrus College

Advanced Camera for Surveys (ACS), Kalas et al. (2008) identified a candidate companion, Fomalhaut b, thought to be consistent with a jovian planet sculpting the debris ring (Chiang et al. 2009) whose emission is at least partially due to a planet atmosphere and circumplanetary accretion. However, sensitive IR observations failed to recover Fomalhaut b (Marengo et al. 2009; Janson et al. 2012), raising doubts about its status as a planet and whether the claimed detection was spurious.

However, in late 2012 Currie et al. (2012a) announced the confirmation of Fomalhaut b, recovering it at a high signal-to-noise in multi-epoch data in filters where Kalas et al. 2008 reported detections – F606W and F814W – and reporting a new ACS detection at F435W. With detections at three filters and new IR upper limits at *J* band ($1.25 \mu m$), Currie et al. (2012a) showed that Fomalhaut b’s emission can be completely explained by scattered starlight from small dust, not thermal emission or accretion, but that this dust is likely bound to a planet-mass body. Soon thereafter, Galicher et al. (2013) independently reported their recovery of Fomalhaut b at the three ACS filters, presented an optical detection from 2010 STIS data¹, and provided additional, sensitive near-IR upper limits using *WFC3*.

While Fomalhaut b is a real object and likely identifies a planet-mass companion, the system may harbor additional planets. In addition to a cold debris ring, Fomalhaut has a warm, asteroid belt analogue located far closer to the star ($\approx 10\text{--}20 AU$; Su et al. 2013; Stapelfeldt et al. 2004). This configuration is similar to that for another A star, HR 8799 (Su et al. 2009), which has debris populations at $\approx 9 AU$ and $\approx 95 AU$ with four directly-imaged planets located at $a_{proj} \approx 15\text{--}70 AU$ between the debris populations (Marois et al. 2010; Currie et al. 2011a). Preliminary results on Fomalhaut b’s astrometry may point to a high eccentricity, ring-crossing orbit due to dynamical perturbations from another planet (Kalas et al. 2013, though see Galicher et al. 2013). Finally, it is unclear whether Fomalhaut b – or another object – is sculpting the debris ring: Janson et al. (2012) identify a candidate point source located interior to Fomalhaut’s debris ring but on the opposite side whose brightness would be consistent with that from a jovian mass companion.

In this Letter, we present new ground-based high-contrast imaging limits on the infrared brightness of Fomalhaut b and a search for the unseen planets responsible for sculpting the host star’s debris belts from $2''$ to $20''$ ($\approx 15\text{--}150 AU$). This work complements recent searches conducted over narrower/smaller ranges in angular separations (Kenworthy et al. 2009, 2013), presenting the first deep constraints on a hypothetical Fomalhaut ‘c’ at $\approx 4\text{--}6''$ or a projected separation of $\approx 30\text{--}45 AU$, similar to the inner two HR 8799 planets *c* and *d*

¹Currie et al. (2012a) also reported a detection of Fomalhaut b in the same STIS data but did not formally present this as a result.

(Marois et al. 2008a).

2. Data

Observations – We downloaded 2002–2005 NIRC2 data from the Keck Observatory Archive (KOA) in the H ($1.65 \mu m$) and L' ($3.8 \mu m$) filters (PIs B. Zuckerman, E. Becklin, and P. Kalas; Table 1) obtained either as a part of the first large ground-based exoplanet imaging surveys (e.g. Kaisler et al. 2005) or as targeted observations of Fomalhaut after the discovery of its debris ring (Kalas et al. 2005). The 2002–2003 Fomalhaut data sets were obtained in classical imaging; others were obtained in *angular differential imaging* (ADI Marois et al. 2006). Kalas et al. (2008) previously report H -band upper limits for Fomalhaut b from Keck/NIRC2 2005 data. The data include those obtained in the wide camera (39.69 mas/pixel) able to identify objects at wide separations like Fomalhaut b and the narrow camera (9.952 mas/pixel; Yelda et al. 2010), sensitive to objects within $\sim 5''$. Basic image processing steps followed previous NIRC2 reductions (Currie et al. 2012b,c). We adopt the narrow camera distortion correction used in Yelda et al. (2010) and the empirically-determined wide camera correction (kindly provided by Hai Fu).

PSF Subtraction – Although the 2002–2003 data were obtained in classical imaging, we nevertheless were able to apply PSF subtraction techniques normally restricted to ADI-mode data (3rd paragraph). Briefly, for alt-az telescopes like Keck, in ADI mode objects located off-axis from a star change in position angle on the detector while quasi-static speckles remain fixed. In classical imaging such objects stay fixed in position while much of the speckle pattern rotates with time. However, the rotation rate of the speckle pattern, like for off-axis point sources in ADI data, is equal to the rate-change of the parallactic angle.

Thus, we can mimick an ADI dataset with frames $i = 1 \dots N_{tot}$ obtained in classical imaging by *rotating* each image i by its change in parallactic angle from the first image: $\delta\theta_i = -1 \times (PA_o - PA_i)$. To realign each image with north-up after PSF subtraction, we *derotate* each image i by the same $\delta\theta_i$, as in a normal ADI data set. Applying this method, we partially suppress quasi-static speckles and achieve significantly deeper contrast gains than simple unsharp masking, subtraction using a 180-degree rotated PSF, or subtraction with a PSF reference star. This method has been independently and successfully tested, yielding a detection of HR 8799 c from July 2004 NIRC2 classical imaging data presented in Marois et al. (2008a) (C. Marois, 2013 pvt. comm.) and can be applied to numerous KOA classical imaging data to identify new planets.

For PSF subtraction, we explored several approaches. For the H -band data and regions

beyond $3''$ in the L' data we used $A - LOCI$ with default values of a large rotation gap ($\delta = 1.5-3$), a large optimization area ($N_A=300-500$) and a weak *singular value decomposition* (SVD) cutoff of 10^{-6} (see Lafrenière et al. 2007; Marois et al. 2010b; Currie et al. 2013, for definitions). For the inner $3''$ of the L' data, we achieved a slight further gain using smaller optimization areas, while adding pixel masking and speckle filtering (Currie et al. 2012a) and retaining the same SVD cutoff.

Photometric Calibration – To flux-calibrate the H and L' data and derive contrast limits, we calculate the brightness of Fomalhaut A observed through the mask in an aperture equal to the measured FWHM and correct for the pupil mask’s extinction. For the H -band data, we adopt the extinction estimate from Metchev et al. (2004) of 7.79 ± 0.22 mags. We derive the L' coronagraph extinction from comparing the brightness of Fomalhaut as observed through the mask to the A-type star SAO 183818, which was observed immediately after Fomalhaut on July 28, 2003 ($m(L') \sim 7.2 \pm 0.1$): $m_{ext}(L') \sim 6.06 \pm 0.15$. We correct for the degradation in our sensitivity due to anisoplanatism from the 2005 H -band data². Finally, we impute artificial point sources into registered images to measure and correct for flux losses from candidate companions due to PSF subtraction and PSF smearing from field rotation (e.g. Lafrenière et al. 2007; Currie et al. 2010).

3. Results

3.1. Reduced Images and Candidate Companions

Figure 1 shows the reduced images obtained for the 2002 H -band data (top-left), 2003 L' data (top-right), the July/October 2005 H -band data (bottom panels). The inner working angles (IWA) for the 2002 and 2005 H -band data are $\approx 2''.3-2''.5$, or $\sim 17.5-20$ AU at Fomalhaut’s distance. The L' data are unsaturated outside of the coronagraph spot and thus are sensitive to companions with separations as small as $0''.5$, or ≈ 4 AU.

We detect seven off-axis objects in total (Table 2). Though the 2002 H -band data are shallow and have only modest speckle suppression, we identify two wide-separation objects (labeled as “1” and “2” in Figure 1, top-left panel). Both 2005 H -band datasets (bottom panels) reveal 5 more objects, at least one, perhaps two of which have small angular extents

²Nominally, we adopt the scaling of Strehl ratio reduction vs. angular distance measured for Keck/NIRC2 from van Dam et al. (2006). For comparison, we measured FWHM along the x and y directions of bright point sources at $r > 10''$ in the 2005 data. The performance reductions are in fair agreement with those noted by Kalas et al. (2008).

consistent with point sources given the PSF undersampling and anisoplanatic effects ($\theta \lesssim 0''.1$). As Fomalhaut b might be extended at red wavelengths (Galicher et al. 2013), the other sources we see could in principle be analogues. At the age of Fomalhaut, the brightnesses of the candidate companions are consistent with $M \sim 5\text{--}15 M_J$ objects (Baraffe et al. 2003; Spiegel and Burrows 2012). The L' data do not clearly reveal any candidate companions within $5''$ of the star (top-right panel). We do not detect any point source at the location of the $\sim 4\text{-}\sigma$ peak identified in Janson et al. (2012) ($[E,N]'' = 6.6, -8.7$).

To establish whether these objects are bound companions, we compare their 2002 and 2005 NIRC2 positions with those from 2004–2006 *ACS* data reduced in Currie et al. (2012a) (Figure 2). We further added 2009 *HST/WFC3* data with basic processing as described in Currie et al. (2012a) and *PSF* subtraction as performed here for Keck/NIRC2 data. We adopt the narrow camera north position angle offset of -0.252° , since there should be no difference here between the narrow and wide cameras (H. Fui, 2013, pvt. comm.): our analysis likewise did not identify clear evidence for an offset. The seven objects have astrometry consistent with that of background objects: the extended sources are then likely background galaxies. Sources 2, 3, and 5 are consistent with previously identified background objects in Currie et al. (2012a); Galicher et al. (2013) also show that an object consistent with Source 3 is a background object and flag Source 5 in their images.

3.2. Limits on Additional Companions and the Near-IR brightness of Fomalhaut b

Contrast Limits – To derive upper limits on the brightness of Fomalhaut b and additional companions, we calculate the dispersion σ in pixel values at a given angular separation (c.f. Marois et al. 2008b) over an aperture area with a two (9.4) pixel diameter for H (L') data to derive the formal $3\text{-}\sigma$ and $5\text{-}\sigma$ contrast and apparent magnitude limit. We combine the 2005 H -band data sets to enhance our point source sensitivity³.

Figure 3 (top-left panel) displays our $3\text{-}\sigma$ contrast limits at H and L' , where magnitude limits can be derived by adding 0.94 to each curve. The L' contrast limit is $\Delta L' \sim 9.3\text{--}11.2$ at the smallest separations ($r = 0''.5\text{--}1''$). Contrast limits for H -band at $r > 13''$ and for L' at $r > 5''$ degrade due to anisoplanatism and poorer sky coverage, respectively. The L' limits

³A bound companion moves too little between epochs to affect our limits at H band. Given Fomalhaut b’s astrometry (Currie et al. 2012a; Galicher et al. 2013), it should move $\approx 0''.02$ between epochs, or \sim half a NIRC2 pixel. Given the PSF broadening at separations where H -band data are more sensitive than L' , this effect is minimal. Three of the four L' data sets were obtained within 2 days of one another.

reach $\Delta L' \sim 15.7$ at $r \sim 3''\text{--}5''$. The H -band limits reach $\Delta H \sim 22.2$ or $m(H) \approx 23.15$ at a range of separations enclosing that of Fomalhaut b and the possible point source reported in Janson et al. (2012) ($10''.75\text{--}13''$). We verified that we can detect planets at our contrast limits. For example, in Figure 3 (top-right panel) we input and recover three artificial point sources into the L' data with brightnesses equal to our estimated $3\text{-}\sigma$ contrast limits at $2''.75$, $3''.15$, and $3''.75$ ($\Delta L' \sim 15.25$, 15.5 , and 15.6).

Planet Detection Limits – To derive mass upper limits from our magnitude limits, we adopt the Hipparcos-measured distance of 7.7 pc , an age of $t = 400\text{--}500\text{ Myr}$ (Mamajek 2012), and the Spiegel and Burrows (2012) (“hybrid clouds”, solar metallicity) and the Baraffe et al. (2003) COND hot-start planet evolution models to map between H and L' magnitudes and planet mass (Figure 3). At Fomalhaut’s age, planet luminosities are independent of the initial entropy (c.f. Spiegel and Burrows 2012). We plot a single curve for each planet cooling model, combining together the H and L' limits. The L' data are deeper at $r \lesssim 5''.2$ ($4''$) for the Spiegel and Burrows (COND) models. We focus on $2''\text{--}20''$ ($r_{proj} \sim 15\text{--}150\text{ AU}$) where we have continuous coverage; Kenworthy et al. (2013) and Meshkat et al. (2013) explore planet mass limits at smaller separations.

The middle and bottom panels of Figure 3 display our mass sensitivity limits at the $3\text{-}\sigma$ (middle) and $5\text{-}\sigma$ (bottom) level assuming ages of 400 Myr (left) and 500 Myr (right) assuming the COND (blue lines) and Spiegel & Burrows (red lines) models. For the COND models, our $3\text{-}\sigma$ upper limits rule out planets with masses $\gtrsim 5\text{--}6\ M_J$ at a projected separation of 15 AU , $\sim 2.5\ M_J$ at 40 AU and $1.5\text{--}2\ M_J$ at $r > 70\text{ AU}$. For the Spiegel and Burrows (2012) models, the corresponding limits are $7\text{--}8\ M_J$ at 15 AU , $5\text{--}6\ M_J$ at 40 AU , and $\sim 4.5\ M_J$ at $r > 70\text{ AU}$. At the $5\text{-}\sigma$ level, our limits are $7\text{--}8\ M_J$ ($8\text{--}9\ M_J$) at 15 AU , $\sim 3\ M_J$ ($5.5\text{--}6\ M_J$) at 40 AU and $1.75\text{--}2\ M_J$ ($4.5\text{--}5\ M_J$) at $> 70\text{ AU}$ assuming the COND (Spiegel & Burrows) models. If the possible point source identified in Janson et al. (2012) is real, then our $5\text{-}\sigma$ limits suggest it must have a mass less than $\sim 1.75\text{--}2\ M_J$ ($4.5\text{--}5\ M_J$) assuming the COND (Spiegel & Burrows) models.

To determine the range of planet masses at $r_{proj} = 15\text{--}150\text{ AU}$ consistent with non-detections reported in the literature, we combine our results with those from Janson et al. (2012) and Kenworthy et al. (2009)⁴. Planets orbiting Fomalhaut comparable in mass and projected separation to HR 8799 bcde ($r_{proj} \sim 15\text{--}70\text{ AU}$) should have been detected. Over most (all) position angles, HR 8799 bcd-like (HR 8799 bc-like) planets in a ring-nested orbit

⁴ For simplicity, we do not include the Kenworthy et al. (2013) limits as they define SNR (and thus contrast) differently than here and in Janson et al. (2012). Kenworthy et al. (2009) state that their data are background limited, not speckle noise limited, over the separations we focus on here ($r > 2''.0$).

($i \sim 66^\circ$, Kalas et al. 2005; Currie et al. 2012a) are detectable in at least one of the data sets. At all projected separations wider than $\sim 45 AU$, we rule out a $M \geq 3 M_J$ planet, comparable to the mass of an object modeled as sculpting Fomalhaut’s debris ring (Chiang et al. 2009).

New IR Detection Limits for Fomalhaut b – We derive a new $3\text{-}\sigma$ upper limit for Fomalhaut b of $m(H) \sim 23.15$, slightly deeper than that derived by Kalas et al. (2008) using the same data, which excludes planets with masses greater than 4–4.5 M_J from the Spiegel and Burrows (2012) models and 1.5–2 M_J from the COND models for an age of 400–500 *Myr*. These limits are comparable to those derived from Spitzer/IRAC, Subaru/IRCS, and *HST/WFC3* (Janson et al. 2012; Currie et al. 2012a; Galicher et al. 2013) and are typically a few tenths of Jupiter-masses lower than reported by Kalas et al. (2008) using a different metric for determining contrast. No current data are sensitive enough to rule out a Jupiter mass for Fomalhaut b, let alone a Saturn.

4. Discussion

Given our mass detection limits, Fomalhaut’s planetary system is now clearly identified as being different than at least some other planetary systems identified from direct imaging. Fomalhaut has apparently failed to form and retain planets at $r_{proj} > 15 AU$ comparable in mass to directly-imaged planets around HR 8799. However, the mass limits we derive near the disk gap edge at most azimuthal angles are significantly deeper than those derived for debris disk-bearing stars in many direct imaging surveys (e.g. Janson et al. 2013). Although Fomalhaut’s planet inventory is different than that of HR 8799, it may be no different than the typical star with a luminous debris disk. Conversely, a Fomalhaut b-like object at typical distances of these disks ($d \approx 30\text{--}50 pc$) would probably be undetectable with any currently-operating instrument. While a planet with a mass/separation comparable to the candidate around HD 95086 (Rameau et al. 2013) would have been detectable, we cannot rule out a β Pic b analogue from our data (Lagrange et al. 2010).

Even though Fomalhaut’s debris ring has been modeled as being sculpted by a super-Jovian mass planet, it is still unclear what determines the ring’s structure. Planets with masses down to 0.5 M_J can sculpt the ring in the Chiang et al. (2009) simulations; perhaps even lower-mass planets located closer to the ring could likewise sculpt it. Planets with masses of 0.5–3 M_J and cold atmospheres at Fomalhaut’s age are likely as faint as $M_H \sim 22\text{--}30$ (Baraffe et al. 2003; Spiegel and Burrows 2012) and thus will be undetectable within the control radius ($r \lesssim 1''$) of next-generation instruments like *SCEXAO*, *GPI*, and *SPHERE* (Martinache and Guyon 2009; Macintosh et al. 2008; Beuzit et al. 2008), although a thermal infrared system like *NaCo* with the *Annular Groove Phase Mask* (Mawet et al.

2013) or *LBTI/LMIRCam* (Wilson et al. 2008) might image slightly more massive companions. Terrestrial mass “shepherding planets” (Boley et al. 2012), which would likewise be undetectable, could also truncate the ring. The ring structure could even have non-planet origins (Lyra and Kuchner 2013) if the ring’s gas-to-dust ratio is near unity.

To shed further substantial light on Fomalhaut’s planet inventory in the next 5–10 years, high-contrast mid-IR imaging with NIRCAM on the *James Webb Space Telescope* will be key (Krist et al. 2007). NIRCAM should achieve a $5\text{-}\sigma$ contrast of $> 10^8$ at $r > 5''$, making even Saturn-mass planets detectable at $r \gtrsim 35$ AU (c.f. Baraffe et al. 2003; Spiegel and Burrows 2012). A NIRCAM non-detection of thermal emission from Fomalhaut b may limit its mass to that of a (Super)-Neptune, a range more consistent with models of circumplanetary dust production from collision between satellites (Kennedy and Wyatt 2011). Fomalhaut b could be the first of many exoplanets studied with *JWST*. NIRCAM’s extreme mid-IR sensitivity will make older ($t \gtrsim 250\text{--}500$ Myr) and/or colder ($T_{\text{eff}} \lesssim 400\text{--}500$ K) Jupiter-mass planets at moderate/wide ($r \sim 1\text{--}10''$) separations around the nearest stars imageable for the first time (Beichman et al. 2010), complementing *GPI/SPHERE/SCEXAO* and later 20-30 m class telescope instrumentation (e.g. Hinz et al. 2012) focused on imaging jovian planets around younger, more distant stars and/or planets at smaller angular separations.

We thank Timothy Rodigas and Mickael Bonnefoy for draft comments; Hai Fu and Stanimir Metchev for discussions regarding the NIRC2 astrometric calibration; Christian Marois for discussions regarding observing techniques; Markus Janson and Matthew Kenworthy for providing their planet detection limits; Chas Beichman for helpful notes on JWST/NIRCAM performance; and Ray Jayawardhana for other helpful comments. This research has made use of the Keck Observatory Archive (KOA), which is operated by the W. M. Keck Observatory and the NASA Exoplanet Science Institute (NExScI), under contract with the National Aeronautics and Space Administration.

REFERENCES

- Acke, B., et al., 2012, *A&A*, 540, 125
- Aumann, H., 1985, *PASP*, 97, 885
- Baraffe, I., et al., 2003, *A&A*, 402, 701
- Beichman, C., et al., 2010, *PASP*, 122, 888
- Beuzit, J.-L., et al., 2008, *SPIE*, 7014, 41

- Boley, A., et al., 2012, *ApJ*, 750, L21
- Chiang, E., et al., 2009, *ApJ*, 693, 734
- Currie, T., Bailey, V., et al., *ApJ*, 2010, 721, L177
- Currie, T., Burrows, A., et al., 2011, *ApJ*, 729, 128
- Currie, T., Thalmann, C., et al., 2011, *ApJ*, 736, L33
- Currie, T., Debes, J., et al., 2012a, *ApJ*, 760, L32
- Currie, T., Fukagawa, M., et al., 2012b, *ApJ*, 755, L34
- Currie, T., Rodigas, T., et al., 2012c, *ApJ*, 757, 28
- Currie, T., Burrows, A., et al., 2013, *ApJ* in press, arXiv:1306.0610
- Galicher, R., et al., 2013, *ApJ*, 769, 42
- Golimowski, D., et al., 2006, *AJ*, 131, 3109
- Hinz, P., et al., 2012, *SPIE*, 8446, 1
- Janson, M., et al., 2012, *ApJ*, 747, 116
- Janson, M., et al., 2013, *ApJ*, 773, 73
- Kaisler, D., 2005, PhD thesis, UCLA
- Kalas, P., et al., 2005, *Nature*, 435, 1067
- Kalas, P., et al., 2008, *Science*, 322, 1345
- Kalas, P., et al., 2013, *ApJ* submitted
- Kennedy, G., Wyatt, M. C., 2011, *MNRAS*, 412, 2137
- Kenworthy, M., et al., 2009, *ApJ*, 697, 1928
- Kenworthy, M., et al., 2013, *ApJ*, 764, 7
- Krist, J., Beichman, C., et al., 2007, *SPIE*, 6693, 16
- Lafrenière, D., et al., 2007, *ApJ*, 660, 770
- Lagrange, A.-M., et al., 2010, *Science*, 329, 57

- Lyra, W., Kuchner, M., 2013, *Nature*, 499, 184
- Macintosh, B., et al., 2008, *SPIE*, 7015, 31
- Mamajek, E., 2012, *ApJ*, 754, L20
- Marengo, M., et al., 2009, *ApJ*, 700, 1647
- Marois, C., et al., 2006, *ApJ*, 641, 556
- Marois, C., et al., 2008a, *Science*, 322, 1348
- Marois, C., et al., 2008b, *ApJ*, 673, 647
- Marois, C., et al., 2010, *Nature*, 468, 1080
- Marois, C., et al., 2010b, *SPIE*, 7736, 52
- Martinache, F., Guyon, O., 2009, *SPIE*, 7440, 20
- Mawet, D., et al., 2013, *A&A*, 552, L13
- Meshkat, T., et al., 2013, *ApJ* submitted
- Metchev, S., et al., 2004, *ApJ*, 617, 1330
- Rameau, J., et al., 2013, *ApJ*, 772, L15
- Spiegel, D., Burrows, A., 2012, *ApJ*, 745, 174
- Stapelfeldt, K., et al., 2004, *ApJS*, 154, 458
- Su, K., et al., 2009, *ApJ*, 705, 314
- Su, K., et al., 2013, *ApJ*, 763, 118
- van Dam, M., 2006, *SPIE*, 6272, 95
- Wilson, J., et al., 2008, *SPIE*, 7013, 101
- Yelda, S., et al., 2010, *ApJ*, 725, 331

Table 1. Observing Log

UT Date	Mode	Camera	R_{mask} (")	IWA (")	Filter	t_{int} (s)	N_{images}	ΔPA (degrees)
2002-08-21	Classical	Wide	1.0	2.3	H	60	21	14.8
2003-07-27	Classical	Narrow	0.5	0.5	L'	45	50	35.3
2003-07-28	Classical	Narrow	0.5	0.5	L'	35	50	28.1
2003-07-29	Classical	Narrow	0.5	0.5	L'	46	50	36.1
2003-08-19	Classical	Narrow	0.5	0.5	L'	40	50	34.1
2005-07-17	ADI	Wide	1.0	2.5	H	30	110	39.2
2005-10-21	ADI	Wide	1.0	2.5	H	30	194	50.8

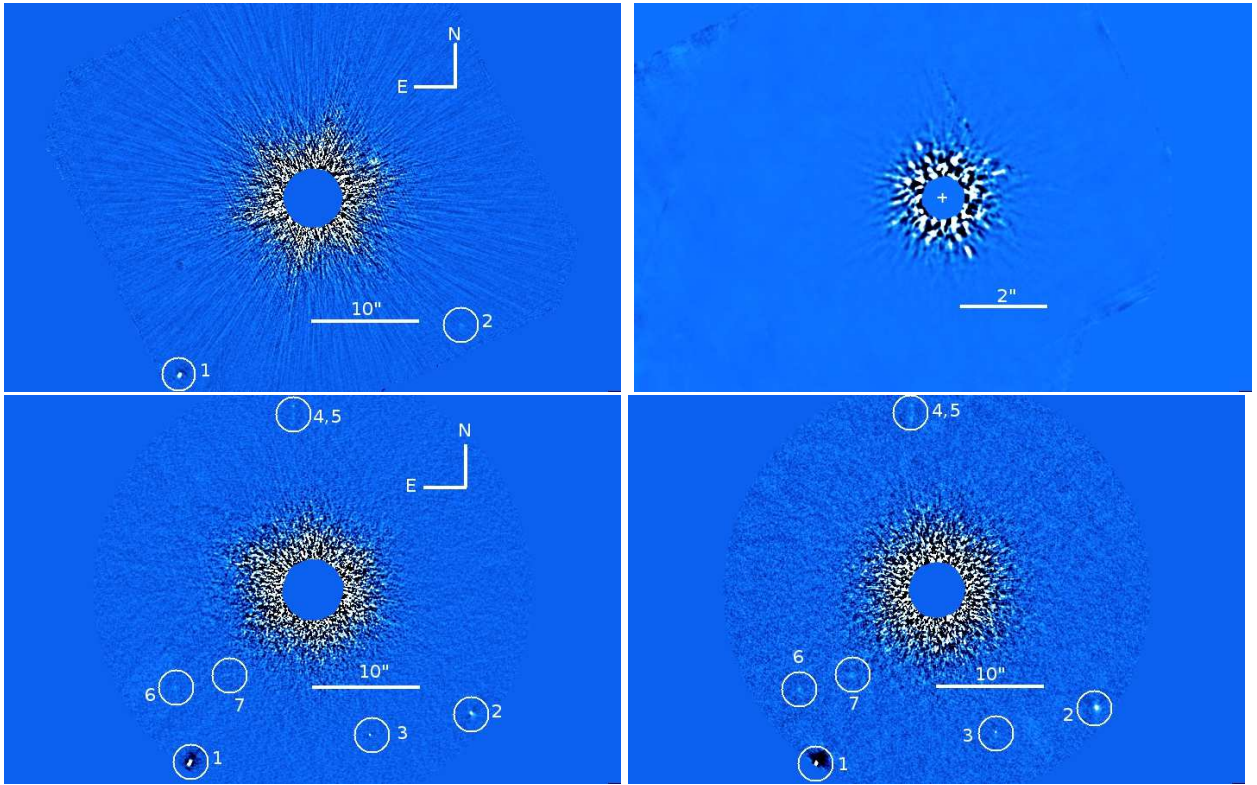


Fig. 1.— Reduced Keck/NIRC2 images (counterclockwise from top-left): 2002 H band data, July 2005 H band data, October 2005 H band data, and July–August 2003 L' data. All images are rotated “north-up” and a horizontal bar denotes the images’ spatial scales. The color stretch in each image is defined to highlight the regions with significant speckle noise contamination. We identify seven off-axis objects in the H band data but none at L' .

Table 2. Candidate Companions Identified from Ground-Based Imaging

Number	Epoch	m_H	[E,N] (")	Extended?	Status?
1	2002-08-21		[12.36,-16.26] \pm 0.04		
	2005-07-17	$< 16.9 \pm 0.2$	[11.36,-15.82] \pm 0.04	yes	bckg
	2005-10-21		[11.44,-15.72] \pm 0.04		
	2006-07-16		[11.01,-15.70] \pm 0.03		
	2009-11-16		[10.20,-15.22] \pm 0.13		
2	2002-08-21		[-13.64,-11.73] \pm 0.04		
	2005-07-17	$< 20.8 \pm 0.2$	[-14.57,-11.34] \pm 0.04	yes	bckg
	2005-10-21		[-14.51,-11.20] \pm 0.04		
	2006-07-16		[-14.96,-11.05] \pm 0.03		
	2009-11-16		[-15.78,-10.55] \pm 0.13		
3	2004-09-26		[-4.86,-13.29] \pm 0.03		
	2005-07-17	21.5 ± 0.2	[-5.25,-13.31] \pm 0.04	no	bckg
	2005-10-21		[-5.16,-13.21] \pm 0.04		
	2006-07-16		[-5.59,-13.11] \pm 0.03		
	2009-11-16		[-6.41,-12.59] \pm 0.13		
4	2005-07-17	$< 22.2 \pm 0.2$	[1.78,16.93] \pm 0.04	yes?	bckg
	2005-10-21		[1.88,17.10] \pm 0.04		
	2009-11-16		[0.67,17.60] \pm 0.13		
5	2005-07-17	$< 22.7 \pm 0.3$	[1.77,15.79] \pm 0.08	yes	bckg
	2005-10-21		[1.82,16.01] \pm 0.08		
	2009-11-16		[0.67,16.56] \pm 0.13		
6	2005-07-17	$< 22.2 \pm 0.3$	[12.72,-8.83] \pm 0.04	yes	bckg
	2005-10-21		[12.80,-8.81] \pm 0.04		
	2009-11-16		[11.58,-8.12] \pm 0.13		
7	2005-07-17	$< 22.4 \pm 0.3$	[7.90,-7.83] \pm 0.04	yes	bckg
	2005-10-21		[7.98,-7.70] \pm 0.04		
	2006-07-16		[7.62,-7.65] \pm 0.06		
	2009-11-16		[6.75,-7.12] \pm 0.13		

Note. — For extended objects, the “ $<$ ” denotes that the magnitude is an upper limit.

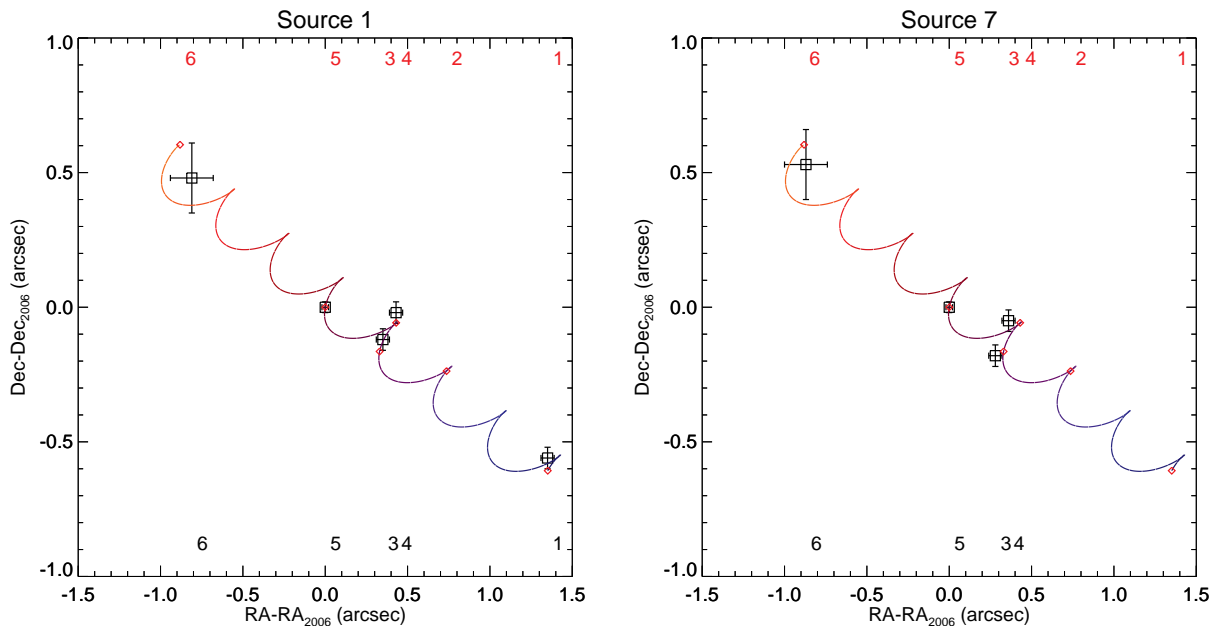


Fig. 2.— Proper motion analysis for sources 1 and 7 listed in Table 2: both plots compare positions to the 2006 *HST* positions from Currie et al. (2012a). Open black squares with error bars denote our measurements; small red squares are the predicted positions for background stars. Combining the Keck data with our reduction of the *HST*/ACS data (Currie et al. 2012a) and WFC3 data (this work) shows that these and all other candidate companions (Table 2) are background objects.

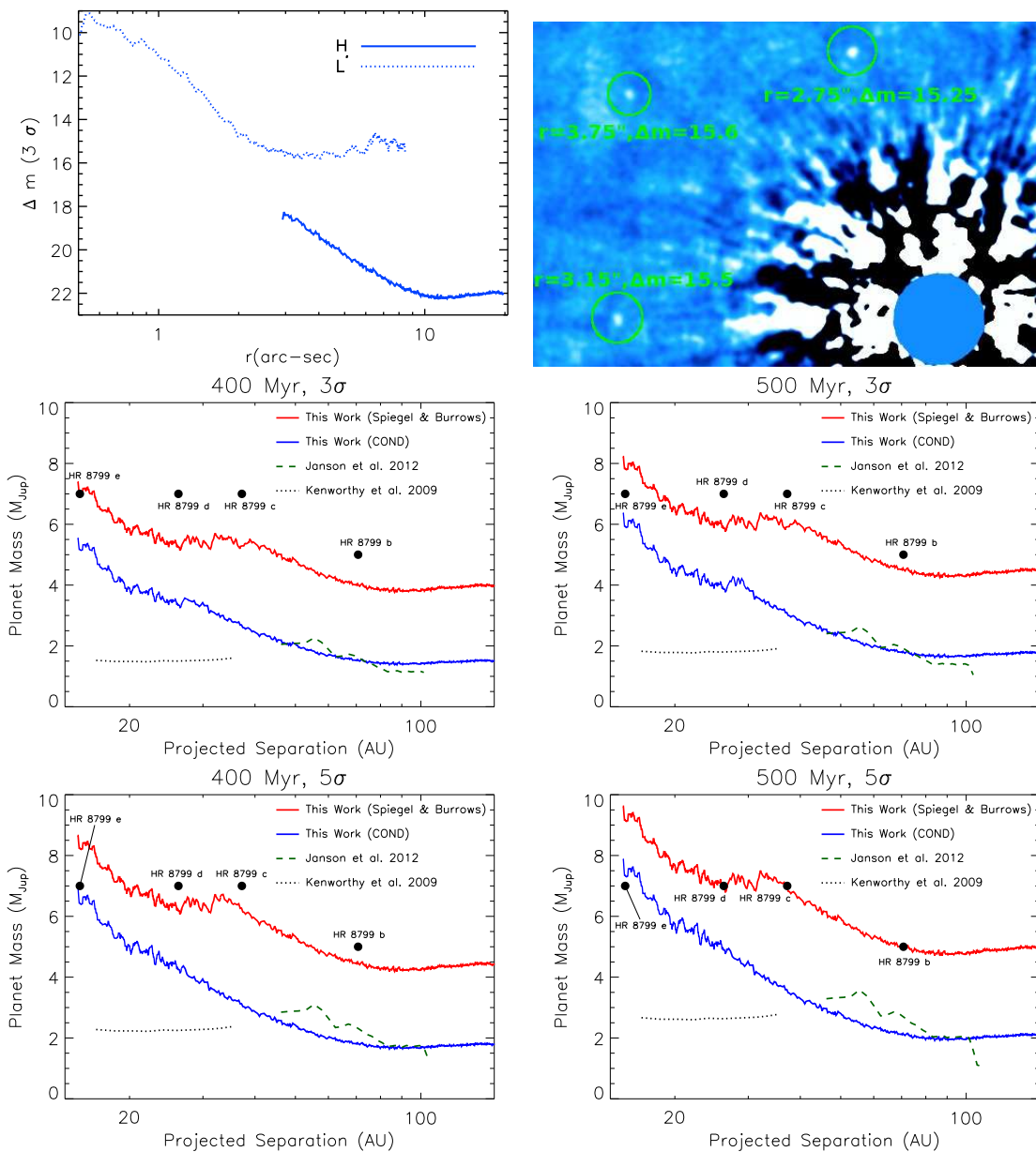


Fig. 3.— (Top-left) Contrast limits (3σ) and tests showing that we can detect planets at these limits (top-right). (Middle and Bottom panels) Our 3σ (middle panels) and 5σ (bottom panels) mass limits assuming an age of 400 *Myr* (left panels) and 500 *Myr* (right panels).